NUCL SCI TECH (2019) 30:27
https://doi.org/10.1007/s41365-019-0551-0

Temperature dependence of CsI:Tl coupled to a PIN photodiode and a silicon photomultiplier

Yu Sun[1,2,3] · Zhi-Yu Sun[1] · Yu-Hong Yu[1] · Ruo-Fu Chen[1] · Shu-Weng Tang[1] · Fang Fang[1] · Duo Yan[1] · Qiang Hu[1] · Ke Yue[1] · Shi-Tao Wang[1] · Xue Heng Zhang[1] · Yong-Jie Zhang[1] · Jun-Lin Chen[1] · Ya-Zhou Sun[1,2,3] · Ze-Hui Cheng[2] · Bi-Tao Hu[2]

Received: 3 July 2018 / Revised: 29 August 2018 / Accepted: 1 September 2018 / Published online: 19 January 2019

Abstract With the aim of simulating the harsh temperature condition of space, a thallium-activated cesium iodide crystal (CsI:Tl) detector readout with a PIN photodiode (CsI:Tl(PD)) and with a silicon photomultiplier (CsI:Tl (SiPM)) is investigated over a temperature range from − 40 to 40 °C. With the increase in temperature, the output signal increases by ∼ 24% with CsI:Tl(PD) and decreases by ∼ 69% with CsI:Tl(SiPM). To reduce the effect of temperature in outer space, a method of bias voltage compensation is adopted for CsI:Tl(SiPM). Our study demonstrates that after correcting the temperature the variation in the analog-to-digital converter's amplitude is $< 3\%$.

Keywords CsI:Tl · SiPM · PD · Temperature dependence · Correction method

This work was supported by the National Natural Science Foundation of China (Nos. 11575257, 11575269, and U1732134) and the Youth Innovation Promotion Association of the Chinese Academy of Science (No. 2015342).

✉ Yu Sun
suny6620661@163.com

Zhi-Yu Sun
sunzhy@impcas.ac.cn

Yu-Hong Yu
yuyuhong@impcas.ac.cn

[1] Institute of Modern Physics, Chinese Academy of Sciences, Lanzhou 730000, China

[2] Lanzhou University, Lanzhou 730000, China

[3] University of Chinese Academy of Sciences, Beijing 100049, China

1 Introduction

In recent decades, because of the increasing interest in outer space, numerous exploration activities have been pursued. The accurate measurement of the space radiation distribution has been regarded as one of the most important tasks during these explorations, because space radiation is harmful to astronauts and electronic devices. Almost all low earth orbit and interplanetary space exploration satellites are equipped with space radiation detectors (SRDs) [1, 2]. Silicon detectors are used as SRDs because they are sensitive to ionizing radiation [3, 4]. However, owing to the limitation of modern semiconductor technology, it is difficult to fabricate them with sufficient thickness that enables them to measure particles with energy up to hundreds of MeV. To reach this measurement goal, silicon hodoscopes are needed. However, employing such devices will increase both power consumption and cost. Consequently, a new tendency in deep space exploration is to use inorganic crystals with high stopping power, such as thallium-activated cesium iodide crystals (CsI:Tl). While the particles are incident on the inorganic crystal, scintillation light can be produced in it. Usually, the signal is read out by photomultiplier tubes (PMTs), which have been widely used in terrestrial experiment, and excellent energy resolution is achieved [5]. Recently, some new photon devices—the silicon photomultiplier (SiPM) and the PIN photodiode (PD)—have been developed and are now widely used [6, 7]. Their specific advantages include their compact volume, low operational voltage, insensitivity to magnetic fields, high photon detection efficiency (PDE), and good optical matching to CsI:Tl. They will enable the next generation of SRDs and will make the whole detection system more compact with lower power consumption. In

contrast to the terrestrial detectors, satellite-borne detectors operate under limited conditions, such as power consumption restrictions, severe launch-dependent constraints on mechanical stability, and good work performance over a wide range of temperatures.

The temperature dependence of the breakdown voltage (V_{bd}) of SiPMs has been widely studied. The typical temperature coefficient of V_{bd} is 40–60 mV/°C, resulting in a gain variation of $\sim$ 3%–45%/°C [8]. To maintain a stable gain for these devices, many ways have been proposed in Refs. [9, 10]. Because the photodetector is made of a scintillator, the light yield can also be influenced by temperature [11, 12]. Up to now, methods to correct for the temperature effect of this combination have been seldom studied. The stability of the gain of SiPMs still limits their application in a variable temperature environment. In this paper, a CsI:Tl manufactured at the Institute of Modern Physics of the Chinese Academy of Sciences is coupled to different readout devices and the temperature dependencies of the amplitude and energy resolutions are studied. Meanwhile, some specific characteristics of SiPMs and PDs are also investigated. In addition, a method for amplitude correction is proposed to reduce the temperature effect. Our study indicates that the method can also be applied to different scintillation detectors.

2 Experimental setup

The scheme of the experimental setup used to study the response of SiPMs and PDs as a function of temperature is shown in Fig. 1a. With the aim of studying the temperature performance of PDs and SiPMs, a blue light-emitting diode (LED) driven by a pulser with variable intensity is used as the light source. Because the light intensity of the LED is temperature dependent [13], therefore, a thermostat room is used to keep the temperature steady. An optical fiber is used to inject the blue light into the photon devices, which are placed in a variable temperature chamber. The optical fiber is fixed to a support frame to eliminate its thermal contraction. The thermal chamber (NT408-70AD, ETOMA Company) has inner dimensions of $700 \times 800 \times 750$ mm^3. It can be operated in a large dynamic temperature range from $-$ 70 to 150 °C. Temperature stability is within $\pm$ 0.5 °C. To avoid condensation of water vapor inside the chamber at low temperature, a dryer system is coupled to the chamber. With the dryer system, dry and clean air can be transported into the thermal chamber to prevent frosting below 0 °C. A PT100 platinum resistance thermocouple is attached to the PD (S3590-08, Hamamatsu Photonics K.K.) [14] or the SiPM (S13360-6050CS, Hamamatsu Photonics K.K.) [15] to monitor the temperature precisely. Their major parameters are listed in Tables 1 and 2, respectively. The power supply, the LED driver, the cables, the electronics, and the data acquisition (DAQ) system are placed outside the thermal chamber, because they are not sensitive to the ambient temperature. The output signal of the PD or SiPM is connected to an amplifier. The unipolar signal from the amplifier is fed into a peak analog-to-digital converter (ADC; V785N, CAEN) [16]. The dipole signal is sent into a fan-in–fan-out module (Phillips 744) to obtain a fast negative signal. Then, the discriminated signal from the constant fraction discriminator (CF8000, ORTEC) is stretched by a logic coincidence module (CO4020, ORTEC) to provide triggers for the ADC. Because the PD has no gain, a charge-sensitive preamplifier (ORTEC 142a) [17] coupled to a spectroscopy amplifier (ORTEC 572A) [18] is adopted to collect the signal produced by the PD. For the SiPM, only a spectroscopy amplifier is used because it has a high gain. Figure 1b represents the experimental setup scheme used to investigate the performance of the CsI:Tl read by the PD or SiPM as a function of temperature. To investigate the temperature effect of a CsI:Tl coupled to a PD and a SiPM, one cube of polished CsI:Tl with a side of 1 cm was coupled to the PD or SiPM through silicone grease. The whole detector was then wrapped with Teflon tape to enhance the reflective efficiency. In addition, the detector was placed in a dark, sealed thermostat and the ambient light was completely blocked by it. A standard radioactive gamma source (^{137}Cs) was used for the test.

3 Results and discussion

3.1 Temperature effects of the SiPM and the PD

To investigate the temperature effect of the PD, a PD with an effective area of 1×1 cm and an optical fiber with a diameter of 1 mm were used. The temperature inside the chamber was allowed to change from $-$ 40 to 45 °C in steps of 10 °C. To guarantee thermal equilibrium between the measured components and the environment, the chamber was kept running for about one hour at each setting temperature before measurements were taken. During the measurement process, the bias voltage of the PD was fixed to 70 V. The ADC peak values of the LED light, which are obtained from a Gaussian fit, as a function of temperature are shown in Fig. 2. The data are fitted with a linear function, as shown in the figure by the red curve. The obtained slope is 2.36 ± 0.04 channel/°C.

By comparing the temperature effect with different devices, the following temperature coefficient can be obtained:

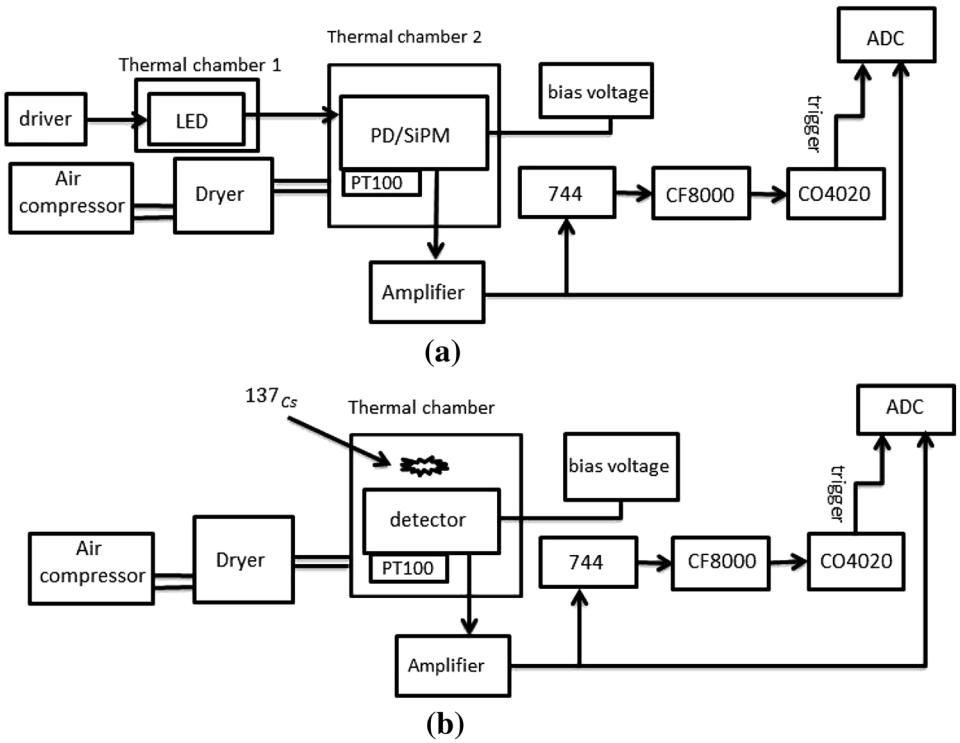

Fig. 1 Sketches of the test equipment. **a** Test setup for studying PD and SiPM performance. **b** Entire test setup

Table 1 Major SiPM parameters

Type	Active area (mm)	Number of pixels	Spectral response range (nm)	Gain	Breakdown voltage (V)	Dark counts (kcps)
S13360-6050CS	6×6	14400	270–900	1.7×10^6	53 ± 3	2000

Table 2 Major PD parameters

Type	Active area (mm)	Spectral response range (nm)	Reverse voltage max (V)	Dark current (nA) $V_R = 70$ V
S3590-08	10×10	340 to 1100	100	2

$$C = \frac{S}{P_{T=20\,^\circ\mathrm{C}}}, \tag{1}$$

where S is the slope and $P_{T=20\,^\circ\mathrm{C}}$ is the ADC channel of the most probable value (MPV) at a temperature of 20 °C [13]. Therefore, the temperature coefficient C of the PD can be calculated by

$$C_{\mathrm{PD}} = (0.097 \pm 0.002)\%/^\circ\mathrm{C}. \tag{2}$$

The measurement process for the SiPM is the same as for the PD. The bias voltage of the SiPM was fixed to 55 V. Figure 3 shows the distribution of the ADC channel of the peak as a function of temperature. A linear function is applied for fitting. The temperature coefficient C of the SiPM is given by

$$C_{\mathrm{SiPM}} = (-1.76 \pm 0.05)\%/^\circ\mathrm{C}. \tag{3}$$

From Figs. 2 and 3, it can be clearly seen that C_{PD} and C_{SiPM} have different signs. The reason why PD has a positive temperature coefficient is that the average ionization energy of electron–hole pairs in the PD decreases when the temperature increases [29]. The opposite tendency for the SiPM may be caused by the increase in the gain of the SiPM with decreasing temperature [19]. The obtained C_{SiPM} is a factor of $\sim 18 > C_{\mathrm{PD}}$, which indicates that the SiPM is more sensitive to temperature than the PD.

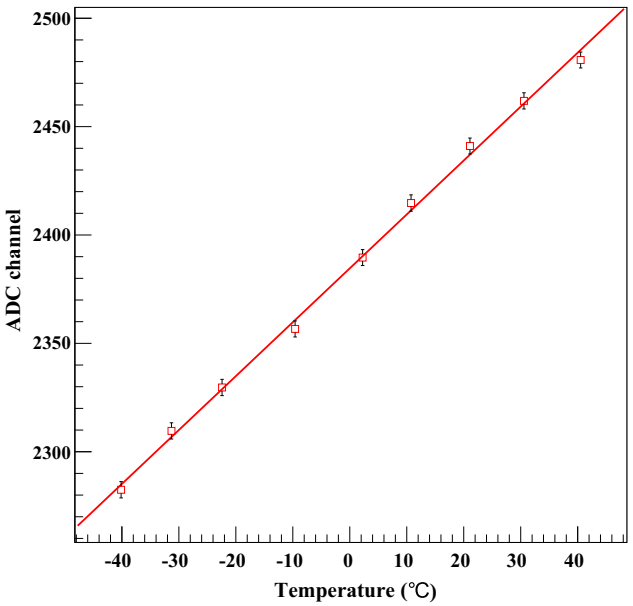

Fig. 2 PD response (ADC channel units) to LED blue light as a function of temperature. The error bars represent the 1σ range of the Gaussian fit

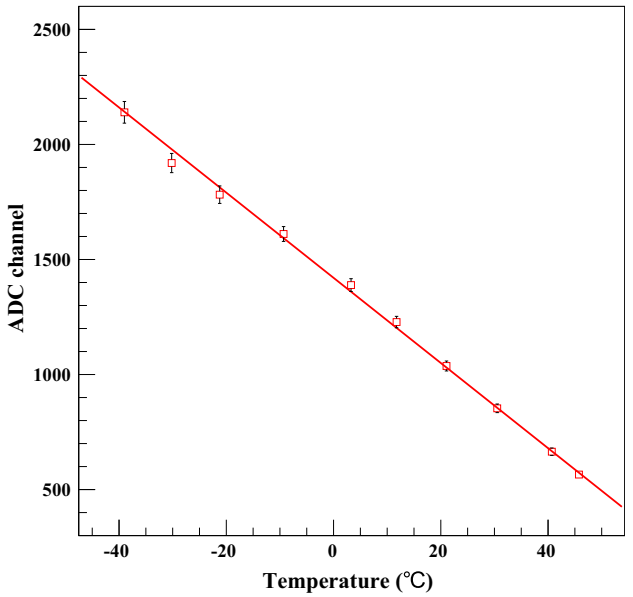

Fig. 3 Distribution of the ADC channel of the peak as a function of temperature (readout with a SiPM). The error bars represent the 1σ range of the Gaussian fit

3.2 Temperature performance of CsI:Tl coupled to a PD a SiPM

The temperature dependencies of CsI:Tl(PD) and CsI:Tl(SiPM) were measured with a ^{137}Cs source at several temperature values from -40 to 45 °C. To reduce the influence from thermoluminescence of the CsI:Tl crystal [20], the thermal chamber was initially heated to 50 °C and then gradually cooled to the set value. Figure 4 shows typical energy spectra at room temperature (20 °C) for CsI:Tl(PD) (Fig. 4a) and CsI:Tl(SiPM) (Fig. 4b). The total energy peak of 662 keV and backscattering peak of 184 keV can be seen clearly in both spectra. Furthermore, the total energy peak in Fig. 4b is much narrower than that in Fig. 4a, indicating that CsI:Tl(SiPM) has better energy resolution than CsI:Tl(PD). The peak of 32 keV is clearly observed for the SiPM readout, but it is mixed with noise for the PD readout, demonstrating that the CsI:Tl crystal coupled to the SiPM has a better signal-to-noise ratio. Therefore, the CsI:Tl crystal coupled to the SiPM has the capability of detecting particles with much lower energy than the CsI:Tl crystal coupled to the PD.

For CsI:Tl crystal readout with the PD, the distribution of the full energy peak (662 keV) as a function of temperature is shown in Fig. 5a. The data shown in the plot have normalized to $T = 20\,°C$. One can see a positive correlation below 20 °C. Saturation is reached somewhere between 20 and 40 °C. The MPV increases by $\sim$ 24 %as the temperature changes from $-$ 40 to 40 °C, which is consistent with the previous result [20]. The experiment shows that the temperature instability of CsI:Tl(PD) mainly comes from the crystal itself, because the contribution of the PD is only 8.8%. Figure 5b shows the relationship between MPVs of the full energy peak (662 keV) and the bias voltages. The test was performed under room temperature (20 °C), and all data have been normalized to $V = 70$ V. It can be clearly seen that, with increase in the bias voltage, the MPVs become almost constant. The reason for this is that the PD reaches full depletion at $\sim$ 70 V [14].

The temperature and bias voltage dependencies of the output amplitude of the CsI:Tl crystal coupled to the SiPM are shown in Fig. 6. With the increase in temperature, the output amplitude varies linearly, which is similar to the

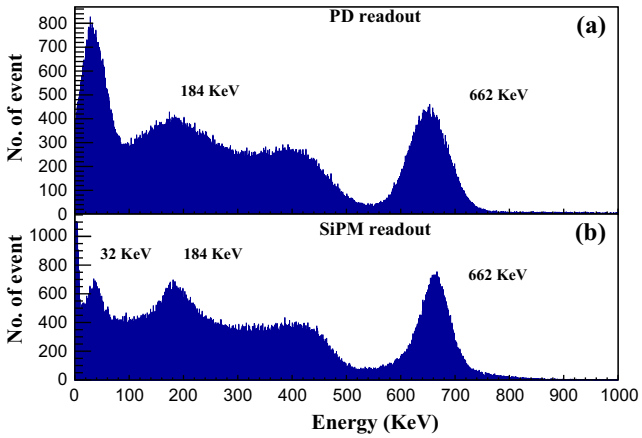

Fig. 4 Energy spectra of the ^{137}Cs source obtained with a CsI:Tl crystal coupled to a PD (**a**) and a SiPM (**b**)

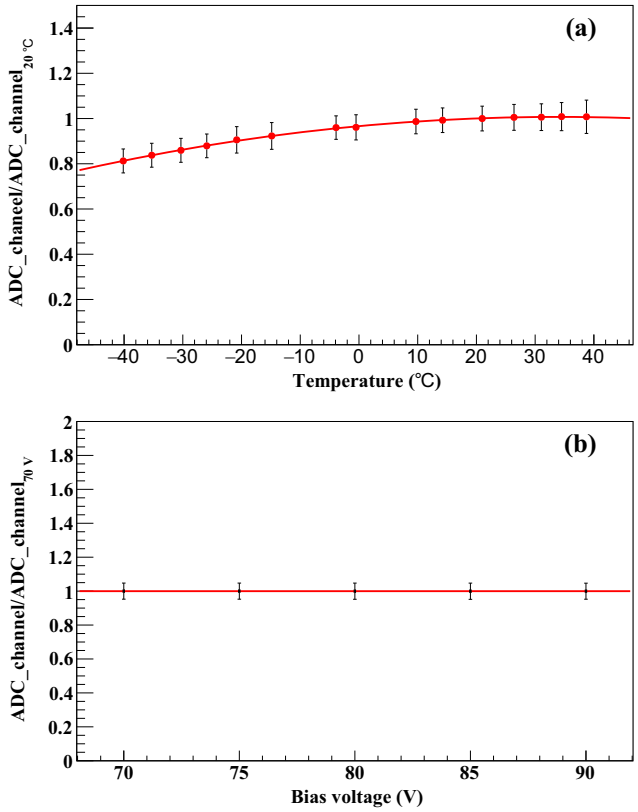

Fig. 5 Relative values of full energy peak of the ^{137}Cs source obtained from a CsI:Tl crystal coupled to a PD at different **a** temperatures and **b** bias voltages. The error bars are the 1σ ranges of the Gaussian fit

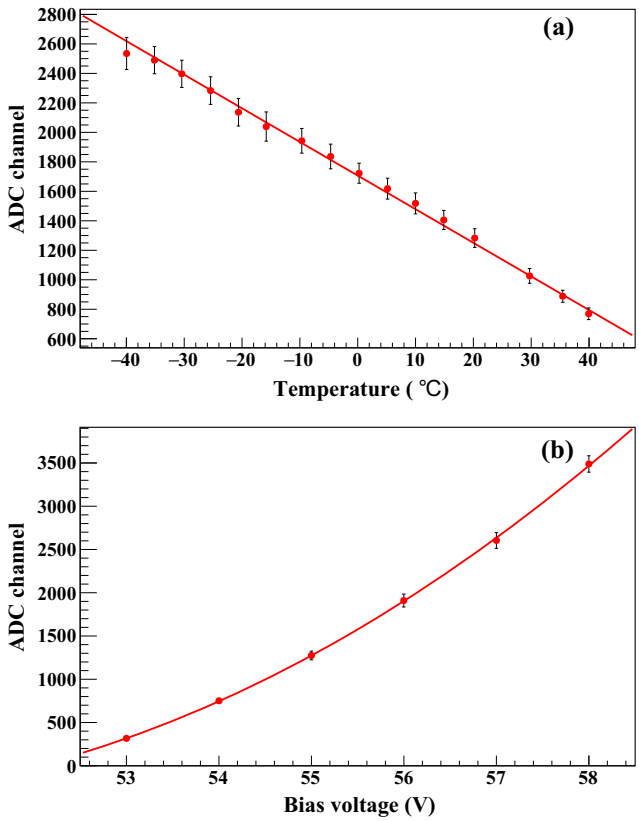

Fig. 6 MPVs of the full energy peak of the ^{137}Cs source obtained from a CsI:Tl crystal coupled to a SiPM at **a** different temperatures and **b** different bias voltages. The bias voltage of the SiPM in (**a**) is set to 55 V. A linear function and a quadratic polynomial function were used to fit the data. The error bars are the 1σ range of the Gaussian fit

observation that can be made from Fig. 3. From 40 to − 40 °C, the output amplitude decreases by ∼ 69%. The temperature coefficient is ∼ − 1.82%, which is close to C_{SiPM}. Therefore, the changes with temperature for this combination are mainly caused by the SiPM. However, a small deviation from linearity is observed at − 40 °C. The reduction in light in the CsI:Tl crystal may be the reason for this deviation. Figure 6b shows the relationship between MPVs of the full energy peak (662 KeV) and the bias voltage of the SiPM. At room temperature (20 °C), the ADC peak position versus bias voltage follows a quadratic polynomial relationship. In the case of constant PDE, the dependence should be linear, whereas the PDE improves with increasing bias voltage. [21] It can be seen that the gain of the SiPM is strongly dependent on the bias voltage, which gives an effective way to correct the temperature effect of the CsI:Tl crystal coupled to the SiPM system.

3.3 Temperature behavior of energy resolution

In this section, the temperature dependence of the CsI:Tl detector's energy resolution is studied. The (width half maximum) energy resolution of the full energy peak can be expressed, following Ref. [21], as

$$(\Delta E/E)^2 = (\delta_{\mathrm{SC}})^2 + (\delta_{\mathrm{ST}})^2 + (\delta_{\mathrm{N}})^2, \quad (4)$$

where δ_{SC} is the crystal's intrinsic resolution, δ_{ST} is the contribution of statistics, and δ_{N} is contributed by the dark noise. Figure 7b shows the distributions of energy resolutions as a function of temperature. The black triangles and red squares are the results of CsI:Tl readout with the SiPM and the PD, respectively. As can be seen, the energy resolutions of CsI:Tl readouts with the SiPM and the PD have similar trends. From − 40 to 40 °C, the relative energy resolutions achieved by CsI:Tl(PD) are ∼ 2% worse than those by CsI:Tl(SiPM). The main reason for this degradation is that the PD has a larger active area and greater dark noise than those of the SiPM at the same temperature. To get better energy resolution, a PD with a proper sensitive area [22] and lower capacitance [23] should be chosen. Figure 7a shows the energy resolutions of the SiPM and the PD as a function of temperature, which are measured with the LED light. In the test, the intensity of the LED light

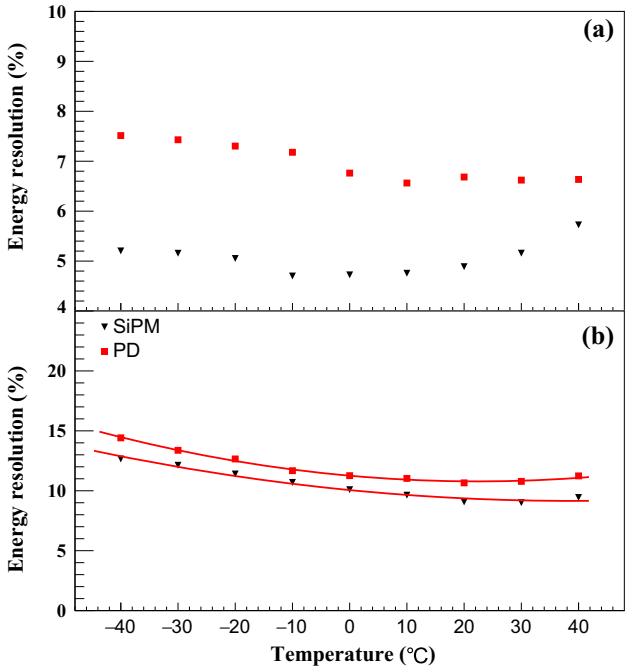

Fig. 7 **a** Energy resolutions as a function of temperature measured with LED light. The black triangles and red squares are the results obtained with a SiPM and a PD, respectively. **b** Comparison of the energy resolution of a CsI:Tl crystal readout with a SiPM and with a PD in the range of − 40 to 40 °C. The error bars in the plot are the 1σ range of the Gaussian fit. The lines in the plot are just used to guide the eye

was adjusted to be comparable with the ones from the CsI:Tl while being irradiated by the ^{137}Cs source. For the test, we obtained energy resolutions of $\sim 5\%$ and $\sim 7\%$ for the SiPM and the PD, respectively. These values are much lower compared to the energy resolution of the CsI(SiPM) system, which is $> 10\%$, as shown in Fig. 7b. In conclusion, the temperature behavior of the energy resolution is dominated by the resolution of the crystal, and small changes in the readout device will not cause significant deviations in the energy resolution. This is consistent with the work in Ref. [24].

Figure 8 presents the energy resolution as a function of the shaping time at room temperature measured for the 662-keV γ rays. For CsI:Tl with the PD readout, the best energy resolution is achieved for a 3-μs shaping time, which means that the best signal-to-noise ratio is obtained at $\sim$ 3 μs of shaping time. For CsI:Tl(SiPM), the detector working with 10 μs can achieve the best energy resolution. The avalanche process of the SiPM will increase the photoelectric collection time. This may be the reason why CsI:Tl(SiPM) has a longer shaping time than CsI:Tl(PD).

As discussed in Sect. 3.2, the output amplitude of a CsI:Tl readout with a SiPM or PD is bias voltage dependent. Further studies show that a detector's energy resolution can also be influenced by the bias voltage, which is

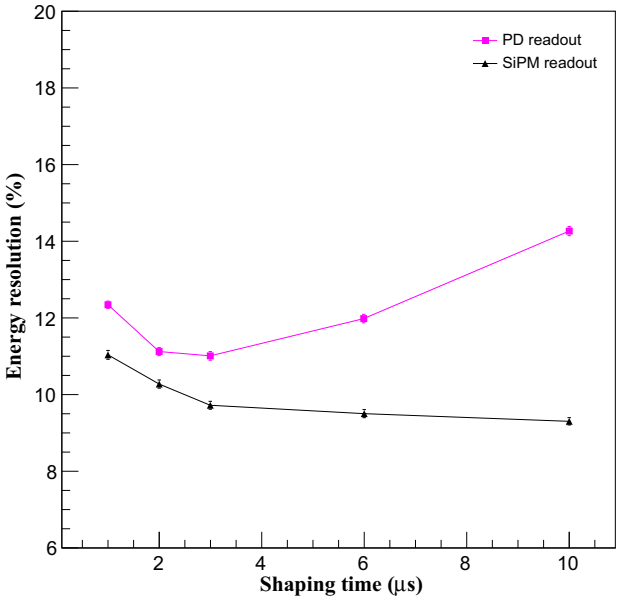

Fig. 8 Total energy resolution as a function of the shaping time measured at room temperature for the 662-keV γ readout with a PD and a SiPM. The error bars in the plot are the 1σ range of the Gaussian fit. The lines in the plot are just used to guide the eye

tested using a standard radioactive source, ^{137}Cs. Figure 9a shows the energy resolution results with the SiPM readout at three different temperatures. For the curve of 45 °C, the energy resolution improves with increasing bias voltage at the beginning. However, as the bias voltage continues to increase, the energy resolution begins to deteriorate. The reason for the improvement in energy resolution is that the PDE becomes greater with the increases in bias voltage.

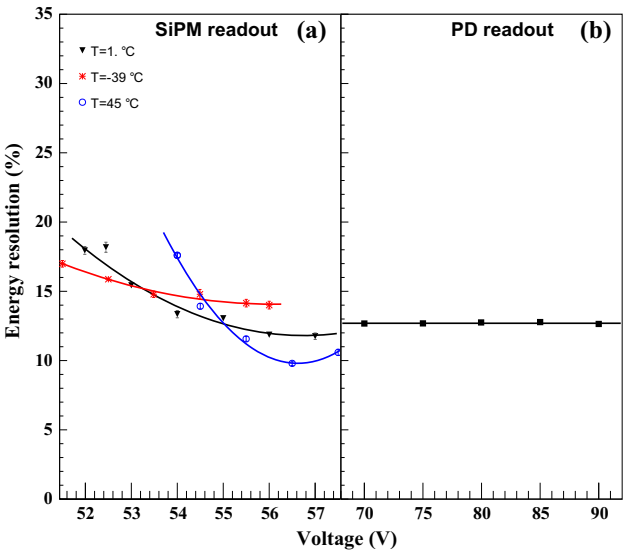

Fig. 9 Distributions of energy resolution as a function of bias voltage at different temperatures for **a** CsI:Tl(SiPM) and **b** CsI:Tl(PD). The error bars in the plot are the 1σ range of the Gaussian fit. The lines in the plot are just used to guide the eye

The deterioration of the energy resolution might be caused by crosstalk and afterpulses of the SiPM. The results are similar to the ones that are shown in Ref. [25, 26]. The other two curves may display the same behavior, but their curves are stopped at too low a voltage value.

Figure 9b shows the results with the PD readout. It is similar to Fig. 5b, with the resolution being almost constant in the test voltage range. This suggests that the noise of the PD does not worsen with the increase in the bias voltage, as described in Ref. [27].

3.4 Correction method

As discussed in the above sections, the CsI:Tl crystal, PD, and SiPM are all temperature dependent, especially the SiPM. Therefore, a method to correct for the temperature effect is necessary for operation of a CsI:Tl readout with a SiPM or PD in a variable temperature environment.

For the PD readout, owing to the small temperature effect, a numerical correction can be adopted. According to previous studies, the following correction function (5) can be used to correct the data back to the temperature of 20 °C:

$$P_a = P_b - p_1 \times (T - 20) - p_2 \times (T^2 - 20^2), \quad (5)$$

where P_b is the raw ADC channel and p_1 and p_2 are the fitting coefficients. The black squares in Fig. 11 show the correction result and a good consistency at different temperatures.

However, for the SiPM readout, a numerical correction is not feasible because the gain of the SiPM is too sensitive to the temperature. A small variation in the temperature may cause a huge change in the dynamic range of the detector. One practical way to solve this problem is to compensate for the gain of the SiPM to reduce the temperature effect with a specific power system. In this manner, the relationship among the gain of the SiPM, the bias voltage, and the temperature can be obtained.

With the data as mentioned above, a three-dimensional drawing can be made, as shown in Fig. 10. To depict the distribution, a surface function is constructed as follows:

$$P = p_0 \times T^2 + p_1 \times T + p_2 \times V^2 + p_3 \times T \times V + p_4 \times V + p_5, \quad (6)$$

where P is the value of the total energy peak, T is the temperature, V is the bias voltage, and p_0, p_1, p_2, p_3, p_4, and p_5 are coefficients that need to be extracted from the fit. According to Eq. (6), by adjusting the bias voltage of the SiPM, the output amplitude can be kept constant at every temperature. To certify the feasibility of this method, a new measurement was performed at different temperatures. The results are shown in Fig. 11 (red inverted triangles). All the

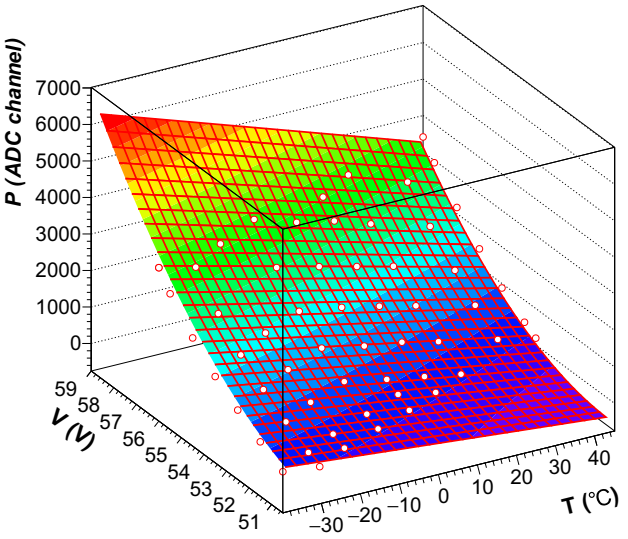

Fig. 10 (Color online) A three-dimensional drawing of the relationship among values of the full energy peaks of the ^{137}Cs source obtained with a CsI:Tl crystal coupled to a SiPM, temperatures, and bias voltages. White points are data, and the colored surface is the fitting result

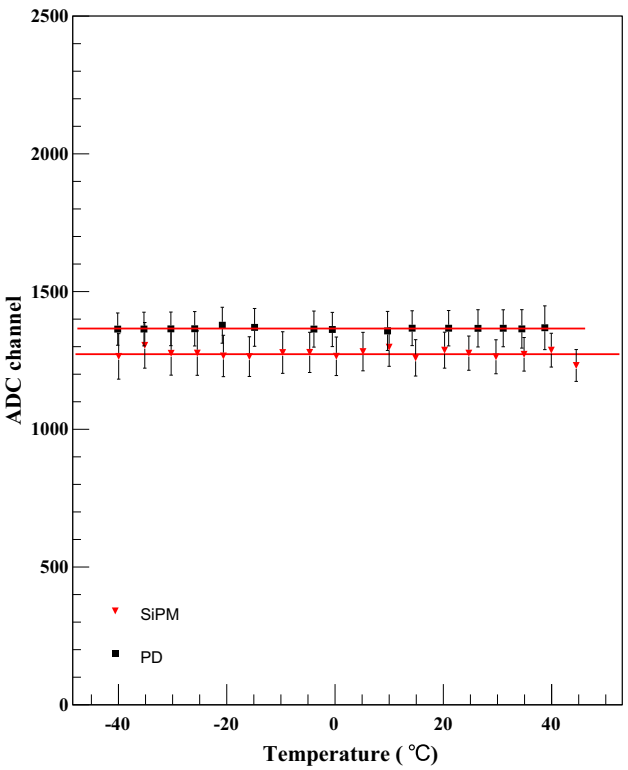

Fig. 11 ADC channels of the full energy peak of the ^{137}Cs source obtained with CsI:Tl(SiPM) (red inverted triangles) at different temperatures after bias voltage compensation. Black squares represent the corrected value for PD readout after numerical correction. The error bars represent the 1σ range of the Gaussian fit

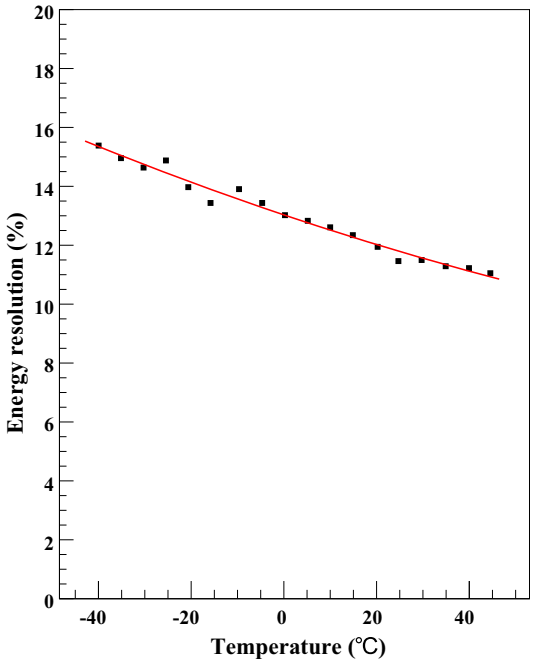

Fig. 12 Energy resolution of the ^{137}Cs source obtained with CsI:Tl(SiPM) as a function of temperature after bias voltage compensation. The line in the figure is just used to guide the eye

data at different temperatures have been corrected to the condition with a bias voltage of $V = 55$ V and a temperature of $T = 20\,^{\circ}$C. A good consistency is achieved with a deviation of $< \pm\ 3\%$. For a possible circuit for adjusting bias voltage with temperature, see Ref. [28]. However, the energy resolution is difficult to improve using this method. Figure 12 shows the distribution of energy resolution as a function of temperature for CsI:Tl(SiPM). It can be observed that, with the increase in working temperature, the energy resolution is improved.

4 Summary

The performances of CsI:Tl(PD) and CsI:Tl(SiPM) are investigated in the temperature range from $-$ 40 °C to 40 °C. The results show that the output signal increases by $\sim 24\%$ for CsI:Tl(PD) and decreases by $\sim 69\%$ for CsI:Tl(SiPM) when the temperature shifts from $-$ 40 °C to 40 °C. The temperature dependence, especially for the SiPM readout, limits the application of this detector in experiments with a wide range of operating temperature, particularly in deep space exploration. Therefore, a numerical method is adopted to correct the temperature effect of CsI:Tl(PD), and a method to compensate for the output by adjusting the bias voltage is implemented to correct for the temperature effect of CsI:Tl(SiPM). Our study shows that the variation in amplitude caused by temperature is suppressed within $\pm 3\%$ for the SiPM readout after correction. In addition, compared to the PD, the maximum number of photons that the SiPM can accept is confined because of its finite number of pixels. Only these particles with energy below a certain threshold can be detected by CsI:Tl(SiPM). Furthermore, the SiPM is more sensitive to temperature than PD. It is a good optical device because of its better energy resolution compared to that of the PD. These two different readout devices have their own advantages, and they can be used for different applications.

Acknowledgements The authors would like to thank Dipika Patal for language revision and helpful suggestions.

References

1. F. Giovacchini, Performance in space of the AMS-02 RICH detector. Nucl. Instrum. Methods A **766**, 57 (2014). https://doi.org/10.1016/j.nima.2014.04.036
2. M. Casolino, V. Bidoli, E. De Grandis et al., Study of the radiation environment in MIR space station with SILEYE-2 experiment. Adv. Space Res. **31**(1), 135–140 (2003). https://doi.org/10.1016/S0273-1177(02)00880-3
3. G.D. Badhwar, P.M. O'Neill, Response of silicon-based linear energy transfer spectrometers: implication for radiation risk assessment in space flights. Nucl. Instrum. Methods A **466**, 464 (2001). https://doi.org/10.1016/S0168-9002(01)00285-6
4. B. Ritter, K. Marsalek, T. Berger et al., A small active dosimeter for applications in space. Nucl. Instrum. Methods A **748**, 61 (2014). https://doi.org/10.1016/j.nima.2014.02.030
5. E. Frlem, D. Pocanic, K.A. Assamagan et al., Design, commissioning and performance of the PIBETA detector at PSI. Nucl. Instrum. Methods A **526**, 300 (2004). https://doi.org/10.1016/j.nima.2004.03.137
6. Q.Y. Wei, T.P. Xu, T.T. Dai et al., Development of a compact DOI-TOF detector module for high-performance PET systems. Nucl. Sci. Tech. **28**, 43 (2017). https://doi.org/10.1007/s41365-017-0202-2
7. B. Aubert, A. Bazan, A. Boucham et al., The BABAR detector. Nucl. Instrum. Methods A **479**, 1 (2002). https://doi.org/10.1016/S0168-9002(01)02012-5
8. N. Dinu, C. Bazin, V. Chaumat et al., Temperature and bias voltage dependence of the MPPC detectors, in *Nuclear Science Symposium & Medical Imaging Conference* (IEEE, 2010), p. 215. https://doi.org/10.1109/NSSMIC.2010.5873750
9. R. Shukla, P. Rakshe, S. Lokhandwala et al., A survey of power supply techniques for silicon photo-multiplier biasing. Int. J. Eng. Res. Gen. Sci. **2**, 599 (2014)
10. R.A. Shukla, V.G. Achanta, S.R. Dugad et al., Multi-channel programmable power supply with temperature compensation for silicon sensors. Rev. Sci. Instrum. **87**, 015114 (2016). https://doi.org/10.1063/1.4940424
11. M. Moszynski, P. CARLSON, Temperature dependence of CsI(Tl) scintillation yield for cosmic muons 5 and 1.25 MeV γ-rays. Nucl. Instrum. Methods A **568**, 739 (2006). https://doi.org/10.1016/0168-9002(89)91234-5
12. J. Valentine, D. wehe, G. knoll, et al., Temperature dependence of absolute CsI(Tl) scintillation yield, in *Nuclear Science Symposium & Medical Imaging Conference* (IEEE, 1991). p. 176. https://doi.org/10.1109/NSSMIC.1991.258897

13. Z.M. Wang, Y.H. Yu, Z.Y. Sun et al., Temperature dependence of the plastic scintillator detector for DAMPE. Chin. Phys. C **41**, 016001 (2017). https://doi.org/10.1088/1674-1137/41/1/016001
14. Hamamatsu Si PIN photodiode. S3590-08/-09/-18/-19 Manual. http://www.hamamatsu.com.cn/UserFiles/DownFile/Product/s3590-08_etc_kpin1052e09.pdf. Accessed 1 Sept 2018
15. Hamamatsu MPPC S13360 series Manual. http://www.hamamatsu.com.cn/UserFiles/DownFile/Product/s13360_series_kapd1052e.pdf. Accessed 1 Sept 2018
16. CAEN V785N Manual. https://www.caen.it/download/?fil ter=V785N. Accessed 1 Sept 2018
17. ORTEC 142A/B/C Preamplifiers Manual. https://www.ortec-online.com/-/media/ametekortec/manuals/142abc-mnl.pdf. Accessed 1 Sept 2018
18. ORTEC 572A Amplifier Manual. https://www.ortec-online.com/-/media/ametekortec/manuals/572a-mnl.pdf. Accessed 1 Sept 2018
19. N. Dinu, Silicon photomultipliers (SiPM), in *Photodetectors: Materials, Devices and Applications*, ed. by B. Nabet (Elsevier, Hoboken, 2016), pp. 255–294. https://doi.org/10.1016/B978-1-78242-445-1.00008-7
20. J.D. Valentine, W.W. Moses, S.E. Derenzo et al., Temperature dependence of CSl(TI) gamma-ray excited scintillation characteristics. Nucl. Instrum. Methods A **325**, 147 (1993). https://doi.org/10.1016/0168-9002(93)91015-F
21. M. Grodzicka, M. Moszynski, T. Szczesniak et al., Energy resolution of small scintillation detectors with SiPM light readout. J. Instrum. **8**, P02017 (2013). https://doi.org/10.1088/1748-0221/8/02/P02017
22. T. Carter, A.J. Bird, A.J. Dean et al., The optimisation of CsI(T1)-PIN photodiode detectors. Nucl. Instrum. Methods A **348**, 567 (1994). https://doi.org/10.1016/0168-9002(94)90802-8
23. H. Grassmann, H.G. Moser, H. Dietl et al., Improvements in photodiode readout for small CsI(Tl) crystals. Nucl. Instrum. Methods A **234**, 122–124 (1984). https://doi.org/10.1016/0168-9002(85)90816-2
24. M. Grodzicka, M. Moszynski, T. Szczesniak et al., Characterization of CsI:Tl at a wide temperature range (− 40 to 20). Nucl. Instrum. Methods A **707**, 73 (2013). https://doi.org/10.1016/j.nima.2012.12.111
25. M. Grodzicka, M. Moszynski, T. Szczesniak et al., MPPC array in the readout of CsI:Tl, LSO:Ce:Ca, $LaBr_3$:Ce, and BGO Scintillators. IEEE Trans. Nucl. Sci. **59**, 6 (2012). https://doi.org/10.1109/TNS.2012.2215343
26. M. Grodzicka, M. Moszynski, T. Szczesniak et al., Characterization of 2*2 ch MPPC array over a wide temperature range (− 20 to 21). J. Instrum. **8**, P07007 (2013). https://doi.org/10.1088/1748-0221/8/07/P07007
27. U. Kilgus, R. Kotthaus, E. Lange et al., Prospects of CsI(Tl)-photodiode detectors for low-level spectroscopy. Nucl. Instrum. Methods A **297**, 425 (1990). https://doi.org/10.1016/0168-9002(90)91325-6
28. F. Licciulli, C. Marzocca, An active compensation system for the temperature dependence of SiPM gain. IEEE Trans. Nucl. Sci. **62**, 228–235 (2015). https://doi.org/10.1109/TNS.2015.2388580
29. B.G. Lowe, R.A. Sareen, A measurement of the electron-hole pair creation energy and the Fano factor in silicon for 5.9 keV X-rays and their temperature dependence in the range 80–270 K. Nucl. Instrum. Methods A **576**, 367 (2007). https://doi.org/10.1016/j.nima.2007.03.020